ACS Partner Journal

CHEMICAL & BIOMEDICAL IMAGING

Open Access

This article is licensed under CC-BY-NC-ND 4.0

pubs.acs.org/ChemBioImaging

Article

Unraveling the Reverse Hofmeister Effect of 3,3′,5,5′-Tetramethylbenzidine for Anion-Responsive Color-Changing Hydrogels

Published as part of Chemical & Biomedical Imaging special issue "Electrochemistry and Imaging".

Yuan Xu, Hong Yang, Kangchun Fu, Yu Liu, Yanfei Shen, Songqin Liu, Yuanyuan He,* and Yuanjian Zhang*

Cite This: https://doi.org/10.1021/cbmi.5c00200

Read Online

ACCESS | Metrics & More | Article Recommendations | Supporting Information

ABSTRACT: Ions are essential regulators of biomolecular stability and function, and their effects are classically summarized in the Hofmeister series. While extensive studies have focused on proteins and other biomacromolecules, whether small molecules exhibit similar ion-specific behaviors remains largely unexplored. Herein, we report the common blue oxidation product of 3,3′,5,5′-tetramethylbenzidine (TMB_{ox1}) as a minimal molecular system that exhibits a reverse Hofmeister effect. In aqueous solution, TMB_{ox1} mimics the key structural features of proteins in terms of terminal amino groups and $\pi-\pi$ stacking motifs and undergoes aggregation in an anion-dependent manner. Combining experiments with the density functional theory and molecular dynamics simulations, we identified the terminal amino groups as key anion interaction sites and $\pi-\pi$ stacking as the intermolecular aggregation interface. MD-based thermodynamic analyses further indicate that chaotropic anions (e.g., I^-) disrupt hydration and shorten $\pi-\pi$ separations, shifting TMB_{ox1} toward denser entropy-favored states. More interestingly, when TMB_{ox1} is confined in an agarose hydrogel, the Hofmeister effect shifts from conventional aggregation to a distinct anion-responsive discoloration. This study demonstrates that small molecules can recapitulate the complex Hofmeister behavior traditionally associated with biomacromolecules. This study provides insights into the molecular determinants of ion-specific effects and highlights their implications for colorimetric sensing and hydrogel-based applications.

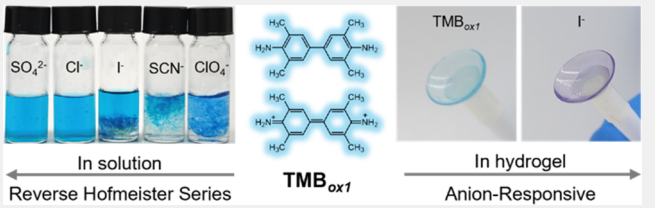

KEYWORDS: *TMB, Hofmeister effect, specific ion effect, colorimetric sensing, nanozyme*

INTRODUCTION

Ions are ubiquitous in living systems, and their task-specific roles are vital for biological processes.[1,2] For instance, sodium is a widespread cation in extracellular fluids that is involved in the regulation of electrolyte balance and blood pressure, while it is much less abundant in the cytosol than potassium. The slightly stronger affinity of sodium for protein than potassium provides clues for the high sodium−low potassium cytosol environment for living organisms.[3] Similarly, chloride is a considerably common biology anion that interacts only weakly with proteins, whereas iodide and certain toxic anions, such as perchlorate and thiocyanate, occur less frequently in biological systems but interact strongly with proteins, particularly in the thyroid, thereby affecting its physiological functions.[4]

Understanding the role of ions in regulating life performance is fascinating at all stages of human history, yet it is subject to the complexity of living systems.[5] A central aspect of life regulation is the maintenance of protein homeostasis, which depends on protein folding, spatial compartmentation, and degradation.[6,7] Thus, the dispersion and aggregation states of proteins are crucial for life performance. In 1880s, Franz Hofmeister first recognized that ions, especially anions, influence protein solubility, giving rise to what is now known as the Hofmeister series.[8,9] Over the past 140 years, the mechanisms underlying the Hofmeister effect have been widely debated, encompassing theories of ion−water interactions, ion−solute interactions, and specific ion effects.[10−13]

The Hofmeister effect has also been reported in other biomacromolecules including DNA, polysaccharides, lipids, and glycoconjugates. For instance, ions can induce conformational twists and structural deformations in DNA.[14] This raises a critical question: do similar ion-specific effects occur in small molecules? Considering that the origin of life is hypothesized to involve simple small molecules, understanding how ions

Received: October 20, 2025
Revised: November 20, 2025
Accepted: November 21, 2025

Downloaded via PURDUE UNIV on December 1, 2025 at 15:38:35 (UTC).
See https://pubs.acs.org/sharingguidelines for options on how to legitimately share published articles.

ACS Publications

© XXXX The Authors. Co-published by Nanjing University and American Chemical Society

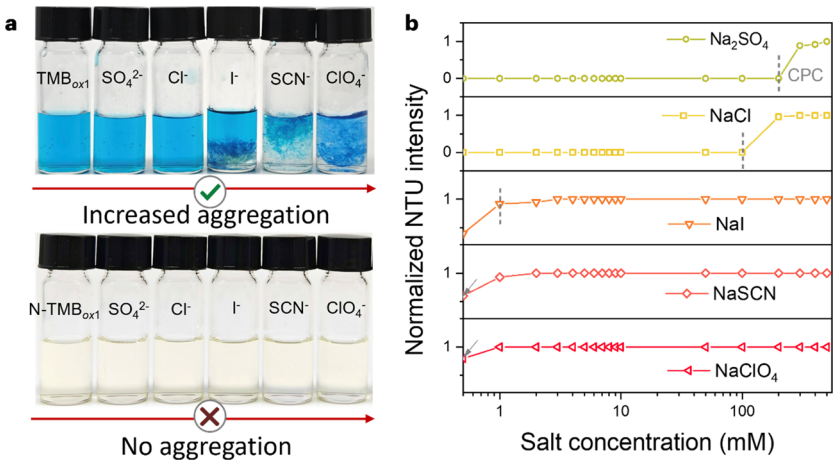

Figure 1. (a) Photographs of TMB_{ox1} after the addition of various sodium salt solutions, arranged according to the Hofmeister series. (b) Normalized NTU intensity for various sodium salt solutions, as measured by the turbidity measurement (NTU: nephelometric turbidity units represent the degree to which the solution obstructs the passage of light). All anion experiments were performed in 0.2 M NaAc/HAc buffer (pH 3.6, $I \approx 0.013$ M), with 2 mM sodium salts added ($I \approx 0.015$–0.019 M) under otherwise identical conditions.

influence their stability may shed light on the emergence of life and deepen our understanding of this fundamental scientific question.

From the perspective of protein structure, two features are particularly important: π–π interactions, which stabilize both proteins and DNA,[15] and terminal amino groups, which play key roles in protein stability and degradation (e.g., the N-end rule pathway).[16] However, to the best of our knowledge, small molecules simultaneously incorporating π–π stacking motifs and terminal amino groups have not been investigated in the context of the Hofmeister effects.

Herein, we report that the one-electron oxidation product of 3,3′,5,5′-tetramethylbenzidine (TMB_{ox1}), bearing π–π stacking interactions and terminal amino groups, exhibits reverse Hofmeister behavior in response to various anions. TMB is a classic colorimetric probe that has attracted enormous interest in colorimetric assays, showing great potential ranging from bioassays to industrial applications owing to its straightforward colorimetric readout.[17−23] This finding has direct implications, highlighting that the ionic environment—particularly counter-anions—must be carefully considered in analytical and industrial applications that rely on colorimetric readouts. To further mimic biological complexity, we confined TMB_{ox1} within an agarose hydrogel network and found that the scope of the Hofmeister effects expanded from simple aggregation in solution to distinct anion-responsive discoloration.

RESULTS AND DISCUSSION

TMB_{ox1}, a one-electron oxidation product of TMB, can be synthesized by using several approaches. We explored two methods and found that TMB_{ox1} exhibited consistent anion-response trends: (i) enzymatic/nanozymatic oxidation using horseradish peroxidase and H_2O_2/nanozymes and (ii) radical oxidation by UV irradiation (365 nm) with superoxide anions (Figure S1).[24] The successful synthesis of TMB_{ox1} by all these methods was validated by UV–vis absorption spectroscopy, showing characteristic peaks at 370 and 652 nm.[25] The nanozyme-catalyzed method was used throughout this study because of its operational simplicity and convenient heterogeneous separation. It is also worth noting that TMB typically exhibits maximum catalytic oxidation kinetics in nanozyme-catalyzed systems at pH 3.6 in acetate–acetic acid buffer, which has been widely adopted in colorimetric assays.[17] Therefore, all experiments in this work were conducted in acetate–acetic acid buffer (pH 3.6) unless otherwise specified.

Upon addition of anions, the TMB_{ox1} solution showed various degrees of aggregation in accordance with the following sequence: $SO_4^{2-} < Cl^- < I^- < SCN^- < ClO_4^-$ (Figure 1a), which is reverse to that of the Hofmeister series; thus, it is termed the reverse Hofmeister effect. In contrast, cations such as sodium and potassium showed negligible effects (Figure S2). To examine the role of the terminal amino group in driving aggregation, N-TMB_{ox}, the oxidized derivative of N,N,N',N'-tetramethylbenzidine that lacks terminal amino groups, was tested as a control in response to different anions. As shown in Figure 1a, aggregation did not occur. To further quantify the reverse Hofmeister behavior of TMB_{ox1}, turbidity measurements were performed to obtain the critical precipitation concentration (CPC) value (Table S1). As illustrated in Figure 1b, the CPC values of TMB_{ox1} after the addition of various anions presented a reverse trend of the Hofmeister behavior. Additional pH-dependent tests confirmed that the aggregation intensity scales with the amount of TMB_{ox1} generated, highlighting the central role of TMB_{ox1} in the observed behavior (Figure S3).

To understand the reverse Hofmeister-like behavior of TMB_{ox1}, it is essential to first clarify its precise molecular structure, which has long been a subject of debate. Historically, the derivation of TMB dates back to 1974, when Holland et al. reported it as a safer substitute for benzidine.[26] In 1981, Bos et al. demonstrated its use as a chromogenic substrate for HRP-based immunoassays.[27] Since then, owing to its low toxicity and high sensitivity, TMB has become the most widely used chromogen in enzyme-linked immunosorbent assay (ELISA).

The oxidation of TMB has been extensively studied by using UV–vis spectroscopy. As shown in Figure 2a, the absorption band at 280 nm corresponds to the TMB diamine structure. Upon one-electron oxidation, TMB_{ox1} is generated, resulting in a characteristic blue color with absorption peaks at 370 and 652 nm. With further oxidation, the band at 280 nm gradually decreased, while TMB_{ox1} accumulated at 370 and 652 nm. At higher oxidation states, a new peak appears at 450 nm, which has been assigned to the two-electron oxidation product (TMB_{ox2}, yellow). Finally, TMB_{ox2} undergoes deprotonation to form $TMB_{ox2'}$ (yellow).

https://doi.org/10.1021/cbmi.5c00200
Chem. Biomed. Imaging XXXX, XXX, XXX–XXX

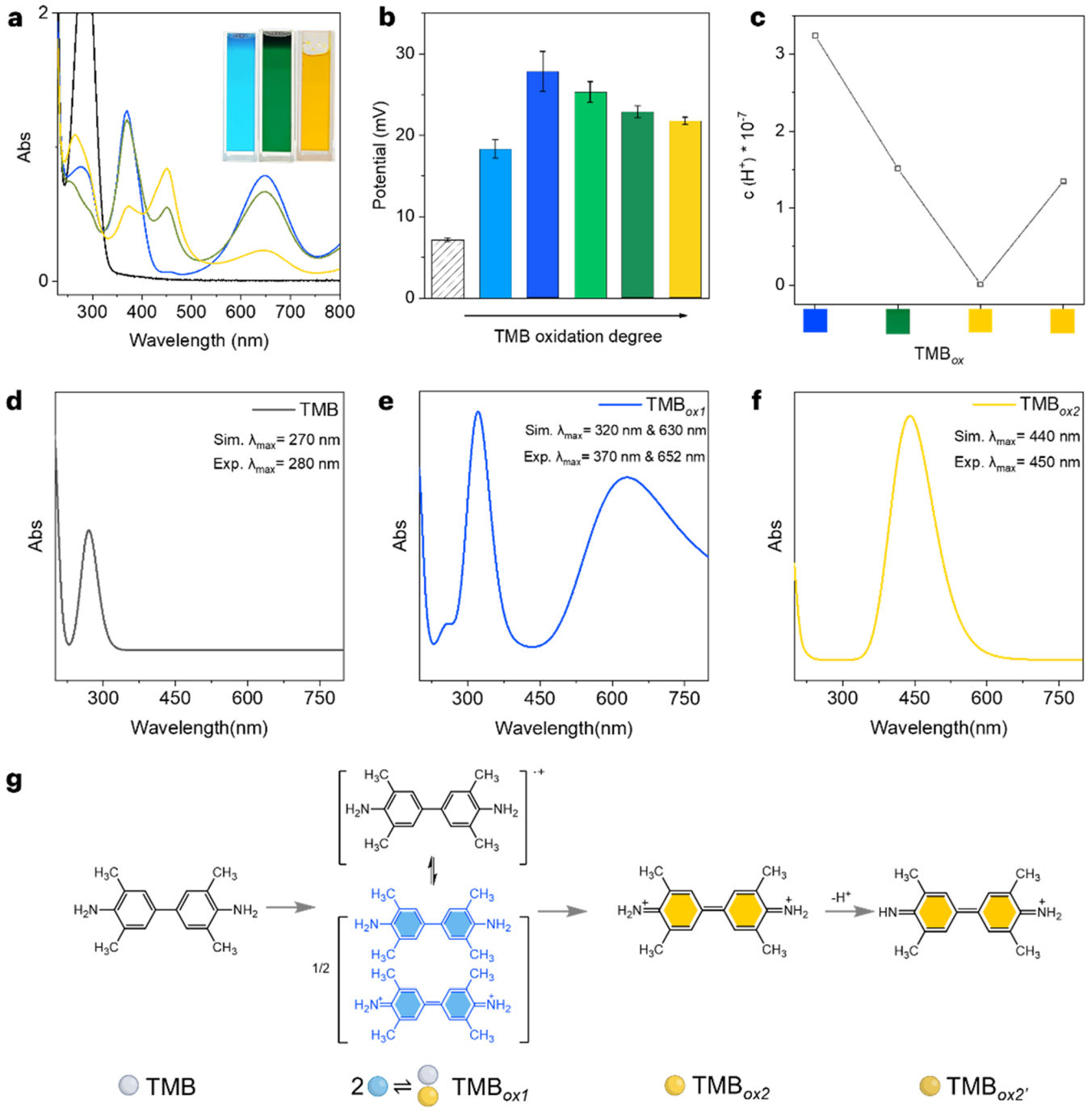

Figure 2. (a) UV−vis spectra of TMB before and after oxidation. (b) Zeta potentials of TMB and the TMB oxidation product. (c) H^+ concentration of TMB and the TMB oxidation product measured using a pH meter. Simulated UV absorption spectra of (d) TMB, (e)TMB_{ox1}, and (f) TMB_{ox2}. (g) Proposed mechanism of TMB oxidation and the molecular structures of each product.

The structure of TMB_{ox1} was initially assigned by Josephy et al. to a semiquinone−imine cation radical in equilibrium with a charge-transfer complex (CTC), based on electron spin resonance and optical spectroscopy.[28] However, the exact nature of this CTC has remained controversial for decades. Two structural models have been proposed: (i) a CTC between the diamine and diimine (denoted as TMB−DTMB), which is widely accepted as the mainstream view, and (ii) a complex between the diamine and diiminium cation (denoted as TMB−TMB^{2+}).[29] Although earlier studies employed various spectroscopic techniques, they were insufficient to unambiguously resolve this structural controversy, and theoretical investigations were largely absent. Despite the widespread application of TMB, the precise molecular structure of its blue oxidation product has not been sufficiently studied.

To address this question, we first examined the charge states and proton involvement in the TMB oxidation. Zeta potential measurements (Figure 2b) revealed that TMB_{ox1} carried positive charges, which increased with the progress of one-electron oxidation. Moreover, pH monitoring (Figure 2c) indicated a gradual decrease in the number of free protons during the TMB_{ox1}-to-TMB_{ox2} conversion, suggesting the involvement of protons in the CTC. Upon the formation of TMB_{ox2}, the number of free protons sharply increased, consistent with the

https://doi.org/10.1021/cbmi.5c00200
Chem. Biomed. Imaging XXXX, XXX, XXX−XXX

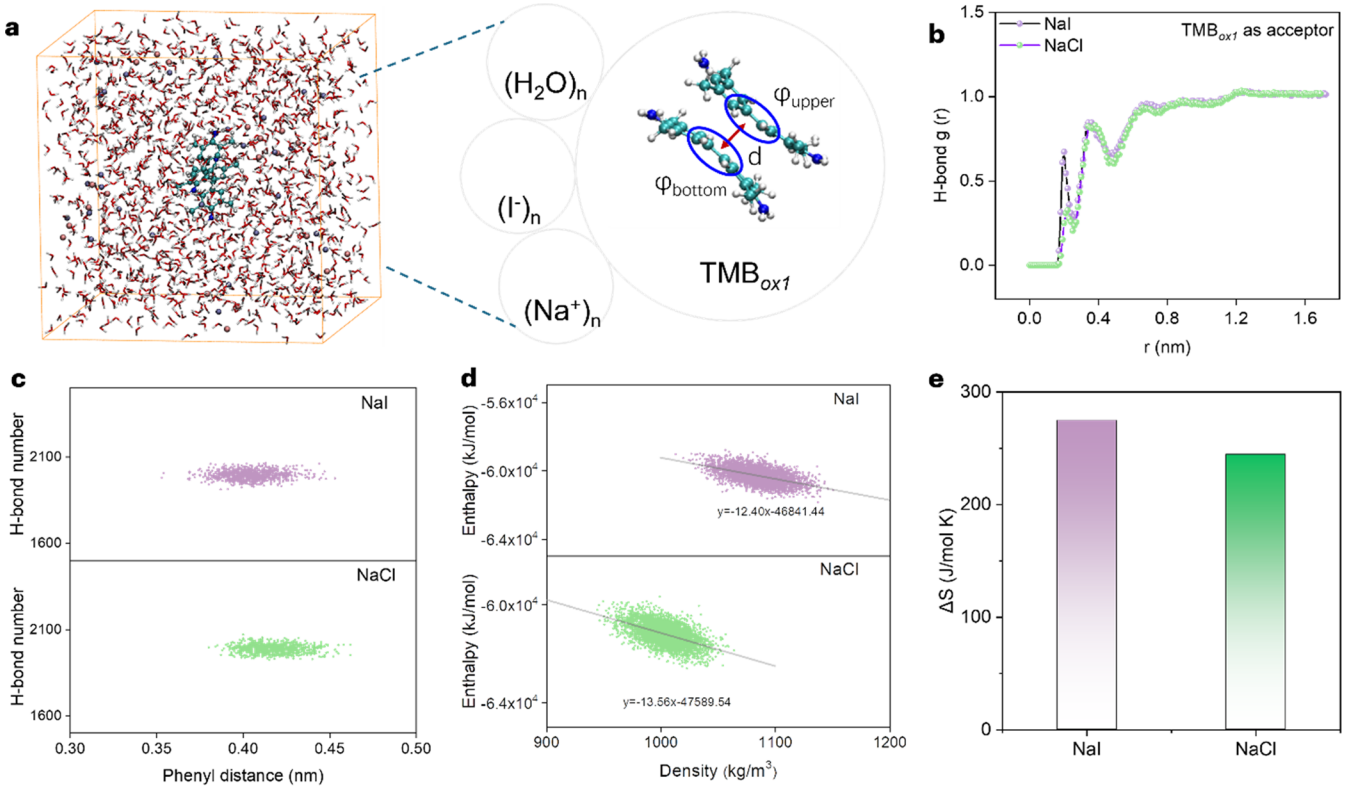

Figure 3. (a) Representative snapshot of the NaI system showing TMB_{ox1} (center) solvated by water molecules, Na^+, and I^- ions. The right panel illustrates the definition of the phenyl−phenyl stacking distance *d* between the upper and lower aromatic rings in the TMB_{ox1} dimers. (b) Radial distribution function $g(r)$ of hydrogen bonds, with TMB_{ox1} acting as a hydrogen-bond acceptor in 1 M NaI and 1 M NaCl solutions. (c) Correlation between the number of hydrogen bonds and the phenyl−phenyl stacking distance for NaI (top) and NaCl (bottom). (d) Correlation between the instantaneous density and enthalpy in the NaI (top) and NaCl (bottom) systems. (e) Comparison of entropy (ΔS) extracted from the MD trajectories.

deprotonation of the two-electron oxidation product. The calculated pK_a values further demonstrated that TMB−DTMB (10.83 and 10.35) has a strong tendency to retain protons, thereby favoring the formation of TMB−TMB^{2+} (Figure S4).

To obtain molecular insights, we conducted density functional theory (DFT) calculations to comprehend the fundamental structures (Figure 2 and S5, TMB, TMB_{ox1}, TMB_{ox2}, and $TMB_{ox2'}$) involved in the oxidation pathway. As shown in Figure 2d,f, the simulated spectra for TMB and TMB_{ox2} align with the experimental data. More importantly, for the one-electron-oxidized intermediate TMB_{ox1}, the simulated absorption of the TMB−TMB^{2+} complex (320 and 632 nm) corresponds more closely to the experimental spectrum of TMB_{ox1} (370 and 652 nm) than the TMB−DTMB structure (263 and 460 nm) (Figure 2e). In addition, thermodynamic calculations indicated that TMB−TMB^{2+} was more energetically favorable than TMB−DTMB (Figures S6 and S7). These findings are corroborated by a few earlier studies that employed electrochemical and spectroscopic methods.[30] Thus, by the theoretical and experimental re-evaluation of TMB_{ox1}'s structure, we determined that TMB−TMB^{2+} is a more logical and consistent structure for the well-known blue product TMB_{ox1} assignment (Figure 2g).

To elucidate why TMB_{ox1} undergoes anion-dependent aggregation, we first examined whether electrostatic interactions could serve as the primary driving force. Considering that TMB_{ox1} carries positive charges, the electrostatic potential (ESP) of the anions was calculated using DFT on the 0.001 au electron density isosurface (Figure S8). The ESP values followed the order SO_4^{2-} < Cl^- < SCN^- < ClO_4^- < I^-, which correlated positively with the experimentally observed aggregation tendency (SO_4^{2-} < Cl^- < I^- < SCN^- < ClO_4^-). This correlation suggests that electrostatics may partly account for the observed Hofmeister sequence. However, the precipitation strength cannot be solely rationalized by electrostatics because kosmotropic anions (e.g., SO_4^{2-} and Cl^-) are strongly hydrated and less effective in approaching TMB_{ox1}, whereas chaotropic anions (e.g., I^- and SCN^-) are weakly hydrated and therefore more prone to induce aggregation. To further test whether the positive charges of TMB_{ox1} alone dictate anion specificity, we investigated TMB_{ox2}, which bears a similarly positively charged group. Figure S9 shows that only minor perturbations were observed even upon the addition of strongly perturbing anions I^-. These observations indicate that additional structural factors are involved.

To probe the microscopic hydration environment, molecular dynamics (MD) simulations were performed using Cl^- and I^- as representative kosmotropic/chaotropic ions (Figure 3a). When TMB_{ox1} acts as a hydrogen-bond donor (TMB−H···Ow), the radial distribution function profiles in Figure 3b for NaCl and NaI nearly overlap, indicating negligible changes in hydration. In contrast, in the acceptor channel, defined as Hw···N_{TMB} (Figure S10), NaI yielded a sharper first-shell $g(r)$ peak at ≈0.2 nm and a reduced outer-shell $g(r)$ intensity across 0.45−0.65 nm, consistent with more localized hydration around the terminal amine nitrogen. This result highlights the terminal amine group as a key interaction site perturbed by chaotropic ions.

We then examined the influence of anions on the intermolecular organization of TMB_{ox1}. The analysis of the correlation between the hydrogen-bond count and phenyl−

https://doi.org/10.1021/cbmi.5c00200
Chem. Biomed. Imaging XXXX, XXX, XXX−XXX

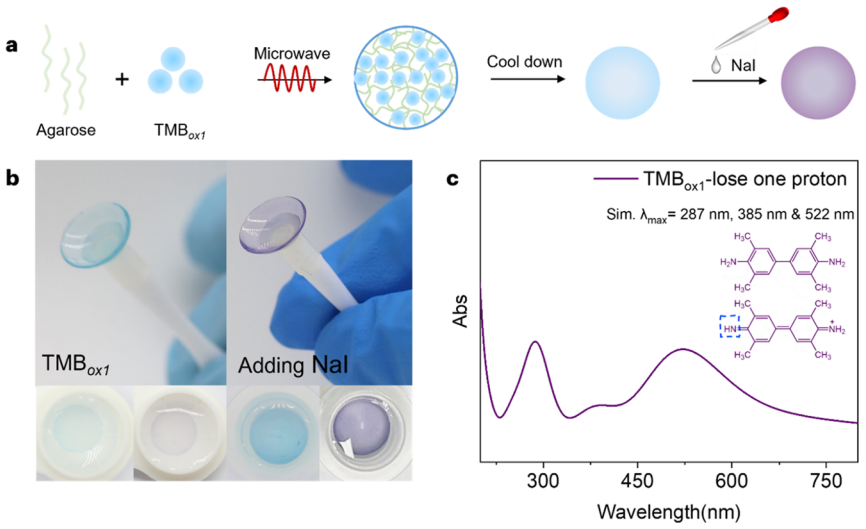

Figure 4. Anion-induced discoloration of TMB$_{ox1}$ hydrogels. (a) Scheme of the preparation procedure of TMB$_{ox1}$@gel by incorporating TMB$_{ox1}$ into an agarose hydrogel and the subsequent color change from blue to purple upon the addition of I^-. (b) Photographs showing the appearance of TMB$_{ox1}$@gel before (blue) and after the addition of NaI (purple) at low (left) and high (right) TMB$_{ox1}$ concentrations. (c) Simulated UV−vis absorption spectrum of TMB−TMB$^+$.

phenyl stacking distance (Figure 3c) revealed that the presence of NaI, as opposed to NaCl, is associated with a population distribution skewed toward shorter $\pi-\pi$ stacking distances. This finding indicates that I^- not only modifies the hydration shell but also enhances the $\pi-\pi$ stacking association of TMB$_{ox1}$ molecules, thereby providing a microscopic rationale for the stronger precipitation observed experimentally. To further evaluate whether the intermolecular distance contributes to anion-specific aggregation, we performed DFT calculations to simulate the absorption spectra of TMB$_{ox1}$ dimers at varying stacking distances. As shown in Figure S11, decreasing intermolecular distance leads to a red shift of the characteristic absorption bands, corresponding to a deeper blue color. This theoretical prediction matches well with the experimental spectral evolution during aggregation (Figure S12), thereby confirming that closer $\pi-\pi$ stacking also plays a critical role in the reverse Hofmeister behavior of TMB$_{ox1}$.

Thermodynamic descriptors were also extracted from the MD trajectories. As shown in Figure 3d, a strong negative correlation exists between the instantaneous density and enthalpy for both NaI and NaCl systems. This indicates that states with higher densities, corresponding to more compact packing, are enthalpically favorable. Notably, the NaI system systematically samples higher density states than NaCl, consistent with the closer $\pi-\pi$ stacking. To further rationalize these thermodynamic trends, qualitative energy decomposition analyses were performed (Figure S13 and Table S2). The results show that the higher density in NaI solutions arises primarily from weakened solute−solvent stabilization rather than stronger solute−solute electrostatics, supporting that chaotropic anions reduce hydration strength and permit tighter molecular association. In addition, quasi-harmonic entropy analysis (ΔS, Figure 3e) indicated a greater increase in the system entropy for NaI than for NaCl. This result supports the mechanism by which chaotropic ions increase the solvent entropy by disrupting the hydration network. Together with the loss of solute configurational entropy upon tighter association, this suggests that the anion-specific aggregation of TMB$_{ox1}$ arises from a balance between enthalpy stabilization and entropic compensation.

In this regard, while electrostatics provide a first-order correlation with the precipitation sequence, MD simulations reveal that chaotropic anions such as I^- perturb both the hydration shell of terminal amines and the $\pi-\pi$ stacking of the CTC, accompanied by thermodynamic signatures of higher density and entropy. These facts explain why TMB$_{ox1}$ exhibits a pronounced Hofmeister-type response, distinct from those of other positively charged species, and underscore the unique role of its terminal amino groups and π-interactions in dictating aggregation.

Among various anions, I^- perturbs hydration, enhances $\pi-\pi$ stacking, and drives TMB$_{ox1}$ toward denser and more entropically favored states. Next, we explored how these microscopic effects manifest in a confined environment. To this end, an agarose hydrogel, a prototypical biological barrier material, was introduced to fabricate the TMB$_{ox1}$@gel (Figure 4a), mimicking a biological network and restricting molecular mobility. Interestingly, in this restricted environment, the typical aggregation behavior of TMB$_{ox1}$ in water was substituted with significant alteration in color and intensity. Initially, TMB$_{ox1}$@gel exhibited a blue hue, but when I^- was introduced, the color transitioned to purple, with the saturation level being influenced by the concentration of TMB$_{ox1}$ (Figure 4b).

DFT calculations were performed to simulate the absorption spectra of the possible structures. As shown in Figure 4c, the simulated UV−vis absorption spectrum of TMB−TMB$^+$ displays characteristic peaks at 287, 385, and 522 nm, which are in good agreement with the experimentally observed purple color. This result shows that the purple color corresponds to a protonated TMB−TMB$^+$ species, in contrast to the blue TMB−TMB^{2+} form. In the hydrogel, the confined environment first restricted the large-scale $\pi-\pi$ stacking and molecular aggregation of TMB$_{ox1}$, thereby stabilizing its monomeric state. Meanwhile, the confined hydrogen-bonding network increased the probability of collisions between I^- and TMB$_{ox1}$, facilitating the removal of a single proton from TMB−TMB^{2+} to yield TMB−TMB$^+$. Consequently, this confinement-assisted deprotonation process was responsible for the color transition from blue to purple. In contrast, no purple color was observed in the bulk solution (Figure S14), as I^-—despite being the

https://doi.org/10.1021/cbmi.5c00200
Chem. Biomed. Imaging XXXX, XXX, XXX−XXX

strongest Brønsted base among common anions ($pK_a = -9$)—typically favors deprotonation without forming a stabilized protonated species.

Taken together, these results demonstrate that the Hofmeister response of TMB_{ox1} is not limited to precipitation in free solution but can also be expressed as anion-specific discoloration under confinement. This anion-responsive color transition extends the scope of traditional stimuli (e.g., temperature, pH, and light) that trigger gel discoloration and provides new molecular-level insights into how terminal amino groups and $\pi-\pi$ stacking interplay with Hofmeister ions to dictate the macroscopic behavior.

CONCLUSION

In summary, we report TMB_{ox1} as a small-molecule model that exhibits reverse Hofmeister behavior, bridging the gap between protein-level observations and molecular-scale mechanisms. Comprehensive experimental and computational results revealed that terminal amino groups act as critical interaction sites for anions, while $\pi-\pi$ stacking governs intermolecular association, together driving anion-specific aggregation in solution. Chaotropic ions, exemplified by I^-, perturb hydration, promote $\pi-\pi$ stacking, and shift the thermodynamic balance toward denser, more entropically favored states. Under confinement within the hydrogel networks, these effects are transformed into a colorimetric response, that is, molecular aggregation of TMB_{ox1} is suppressed, while the strengthened hydrogen-bonding environment facilitates I^--induced deprotonation of $TMB-TMB^{2+}$ to yield the purple $TMB-TMB^{+}$ species, offering a new form of anion-responsive discoloration beyond conventional triggers such as pH, light, or temperature changes. Because the two-electron oxidation product (TMB_{ox2}) can be accelerated by spatial and electrostatic isolation within sodium dodecyl sulfate-based micelles,[31] the present study extends the concept of confined regulation from micellar nanodomains to hydrogel networks. In addition, by validating the molecular spectrum with DFT simulations, we revealed that TMB_{ox1} exists as a CTC between the diamine and diiminium cation ($TMB-TMB^{2+}$), rather than the long-standing structural model between the diamine and diimine (denoted as TMB–DTMB).[28] This structural clarification refines the molecular description of the blue oxidation product and bears practical significance, as TMB-based colorimetric assays are widely used in ionic environments. It thus provides a more reliable basis for interpreting and optimizing TMB-derived sensing systems. These findings not only deepen our understanding of Hofmeister effects at the molecular level but also underscore the importance of considering ionic environments in colorimetric assays and hydrogel systems, with potential implications for both fundamental biochemistry and practical analytical applications.

ASSOCIATED CONTENT

Supporting Information

The Supporting Information is available free of charge at https://pubs.acs.org/doi/10.1021/cbmi.5c00200.

Additional details on chemicals, reagents, characterization methods, material synthesis procedures, and computational methodologies, including DFT calculations and MD simulations (PDF)

AUTHOR INFORMATION

Corresponding Authors

Yuanyuan He − *College of Material and Textile Engineering, Jiaxing University, Jiaxing 314001 Zhejiang, China*; Email: heyy@zjxu.edu.cn

Yuanjian Zhang − *Jiangsu Engineering Laboratory of Smart Carbon-Rich Materials and Device, Jiangsu Province Hi-Tech Key Laboratory for Bio-Medical Research, School of Chemistry and Chemical Engineering, Medical School, Southeast University, Nanjing 211189, China*; orcid.org/0000-0003-2932-4159; Email: Yuanjian.Zhang@seu.edu.cn

Authors

Yuan Xu − *Jiangsu Engineering Laboratory of Smart Carbon-Rich Materials and Device, Jiangsu Province Hi-Tech Key Laboratory for Bio-Medical Research, School of Chemistry and Chemical Engineering, Medical School, Southeast University, Nanjing 211189, China*

Hong Yang − *Jiangsu Engineering Laboratory of Smart Carbon-Rich Materials and Device, Jiangsu Province Hi-Tech Key Laboratory for Bio-Medical Research, School of Chemistry and Chemical Engineering, Medical School, Southeast University, Nanjing 211189, China*

Kangchun Fu − *Jiangsu Engineering Laboratory of Smart Carbon-Rich Materials and Device, Jiangsu Province Hi-Tech Key Laboratory for Bio-Medical Research, School of Chemistry and Chemical Engineering, Medical School, Southeast University, Nanjing 211189, China*

Yu Liu − *Jiangsu Engineering Laboratory of Smart Carbon-Rich Materials and Device, Jiangsu Province Hi-Tech Key Laboratory for Bio-Medical Research, School of Chemistry and Chemical Engineering, Medical School, Southeast University, Nanjing 211189, China*

Yanfei Shen − *Jiangsu Engineering Laboratory of Smart Carbon-Rich Materials and Device, Jiangsu Province Hi-Tech Key Laboratory for Bio-Medical Research, School of Chemistry and Chemical Engineering, Medical School, Southeast University, Nanjing 211189, China*; orcid.org/0000-0003-0369-5920

Songqin Liu − *Jiangsu Engineering Laboratory of Smart Carbon-Rich Materials and Device, Jiangsu Province Hi-Tech Key Laboratory for Bio-Medical Research, School of Chemistry and Chemical Engineering, Medical School, Southeast University, Nanjing 211189, China*; orcid.org/0000-0002-4686-5291

Complete contact information is available at: https://pubs.acs.org/10.1021/cbmi.5c00200

Author Contributions

The manuscript was written through contributions of all authors. All authors have given approval to the final version of the manuscript.

Notes

The authors declare no competing financial interest.

ACKNOWLEDGMENTS

This work was supported by the National Natural Science Foundation of China (22174014, 22074015).

REFERENCES

(1) Zhou, Y.; Morais-Cabral, J. H.; Kaufman, A.; MacKinnon, R. Chemistry of ion coordination and hydration revealed by a K+ channel−Fab complex at 2.0 Å resolution. *Nature* **2001**, *414* (6859), 43−48.

(2) Tobias, D. J.; Hemminger, J. C. Getting Specific About Specific Ion Effects. *Science* **2008**, *319* (5867), 1197−1198.

(3) Vrbka, L.; Vondrasek, J.; Jagoda-Cwiklik, B.; Vacha, R.; Jungwirth, P. Quantification and rationalization of the higher affinity of sodium over potassium to protein surfaces. *Proc. Natl. Acad. Sci. U.S.A.* **2006**, *103* (42), 15440−15444.

(4) Braverman, L. E.; He, X.; Pino, S.; Cross, M.; Magnani, B.; Lamm, S. H.; Kruse, M. B.; Engel, A.; Crump, K. S.; Gibbs, J. P. The Effect of Perchlorate, Thiocyanate, and Nitrate on Thyroid Function in Workers Exposed to Perchlorate Long-Term. *J. Clin. Endocrinol. Metab.* **2005**, *90* (2), 700−706.

(5) Rembert, K. B.; Paterova, J.; Heyda, J.; Hilty, C.; Jungwirth, P.; Cremer, P. S. Molecular mechanisms of ion-specific effects on proteins. *J. Am. Chem. Soc.* **2012**, *134* (24), 10039−10046.

(6) Klaips, C. L.; Jayaraj, G. G.; Hartl, F. U. Pathways of cellular proteostasis in aging and disease. *J. Cell Biol.* **2018**, *217* (1), 51−63.

(7) Alecki, C.; Rizwan, J.; Le, P.; Jacob-Tomas, S.; Comaduran, M. F.; Verbrugghe, M.; Xu, J. M. S.; Minotti, S.; Lynch, J.; Biswas, J.; Wu, T.; Durham, H. D.; Yeo, G. W.; Vera, M. Localized molecular chaperone synthesis maintains neuronal dendrite proteostasis. *Nat. Commun.* **2024**, *15* (1), 10796.

(8) Baldwin, R. L. How Hofmeister ion interactions affect protein stability. *Biophys. J.* **1996**, *71* (4), 2056−2063.

(9) Hofmeister, F. Zur Lehre von der Wirkung der Salze. *Arch. Exp. Pathol. Pharmakol.* **1888**, *24* (4−5), 247−260.

(10) Lin, W.; Zhang, G.; Zhu, X.; Yu, P.; Alimi, L. O.; Moosa, B. A.; Sessler, J. L.; Khashab, N. M. Caging the Hofmeister Effect by a Biomimetic Supramolecular Receptor. *J. Am. Chem. Soc.* **2023**, *145* (23), 12609−12616.

(11) Jordan, J. H.; Gibb, C. L. D.; Wishard, A.; Pham, T.; Gibb, B. C. Ion-Hydrocarbon and/or Ion-Ion Interactions: Direct and Reverse Hofmeister Effects in a Synthetic Host. *J. Am. Chem. Soc.* **2018**, *140* (11), 4092−4099.

(12) Lo Nostro, P.; Ninham, B. W. Hofmeister phenomena: an update on ion specificity in biology. *Chem. Rev.* **2012**, *112* (4), 2286−2322.

(13) Jungwirth, P.; Cremer, P. S. Beyond Hofmeister. *Nat. Chem.* **2014**, *6* (4), 261−263.

(14) Zhang, C.; Tian, F.; Lu, Y.; Yuan, B.; Tan, Z.-J.; Zhang, X.-H.; Dai, L. Twist-diameter coupling drives DNA twist changes with salt and temperature. *Sci. Adv.* **2022**, *8* (12), No. eabn1384.

(15) Wilson, K. A.; Kellie, J. L.; Wetmore, S. D. DNA-protein pi-interactions in nature: abundance, structure, composition and strength of contacts between aromatic amino acids and DNA nucleobases or deoxyribose sugar. *Nucleic Acids Res.* **2014**, *42* (10), 6726−6741.

(16) Varshavsky, A. N-degron and C-degron pathways of protein degradation. *Proc. Natl. Acad. Sci. U.S.A.* **2019**, *116* (2), 358−366.

(17) Jiang, B.; Duan, D.; Gao, L.; Zhou, M.; Fan, K.; Tang, Y.; Xi, J.; Bi, Y.; Tong, Z.; Gao, G. F.; Xie, N.; Tang, A.; Nie, G.; Liang, M.; Yan, X. Standardized assays for determining the catalytic activity and kinetics of peroxidase-like nanozymes. *Nat. Protoc.* **2018**, *13* (7), 1506−1520.

(18) Engvall, E.; Perlmann, P. Enzyme-linked immunosorbent assay (ELISA) quantitative assay of immunoglobulin G. *Immunochemistry* **1971**, *8* (9), 871−874.

(19) Zhang, Y.; Wei, G.; Liu, W.; Li, T.; Wang, Y.; Zhou, M.; Liu, Y.; Wang, X.; Wei, H. Nanozymes for nanohealthcare. *Nat. Rev. Methods Primers* **2024**, *4* (1), 36.

(20) Zeng, R.; Gao, Q.; Xiao, L.; Wang, W.; Gu, Y.; Huang, H.; Tan, Y.; Tang, D.; Guo, S. Precise Tuning of the D-Band Center of Dual-Atomic Enzymes for Catalytic Therapy. *J. Am. Chem. Soc.* **2024**, *146* (14), 10023−10031.

(21) Ji, S. F.; Jiang, B.; Hao, H. G.; Chen, Y. J.; Dong, J. C.; Mao, Y.; Zhang, Z. D.; Gao, R.; Chen, W. X.; Zhang, R. F.; Liang, Q.; Li, H. J.; Liu, S. H.; Wang, Y.; Zhang, Q. H.; Gu, L.; Duan, D. M.; Liang, M. M.; Wang, D. S.; Yan, X. Y.; Li, Y. D. Matching the kinetics of natural enzymes with a single-atom iron nanozyme. *Nat. Catal.* **2021**, *4* (5), 407−417.

(22) Li, S. R.; Zhang, Y. H.; Wang, Q.; Lin, A. Q.; Wei, H. Nanozyme-Enabled Analytical Chemistry. *Anal. Chem.* **2022**, *94* (1), 312−323.

(23) Zhang, R.; Yan, X.; Gao, L.; Fan, K. Nanozymes expanding the boundaries of biocatalysis. *Nat. Commun.* **2025**, *16* (1), 6817.

(24) Xu, Y.; Ma, Y.; Chen, X.; Wu, K.; Wang, K.; Shen, Y.; Liu, S.; Gao, X.; Zhang, Y. Regulating Reactive Oxygen Intermediates of Fe−N−C SAzyme via Second-Shell Coordination for Selective Aerobic Oxidation Reactions. *Angew. Chem., Int. Ed.* **2024**, *63* (36), No. e202408935.

(25) Zhang, X.; Yang, Q.; Lang, Y.; Jiang, X.; Wu, P. Rationale of 3,3′,5,5′-Tetramethylbenzidine as the Chromogenic Substrate in Colorimetric Analysis. *Anal. Chem.* **2020**, *92* (18), 12400−12406.

(26) Holland, V. R.; Saunders, B. C.; Rose, F. L.; Walpole, A. L. A safer substitute for benzidine in the detection of blood. *Tetrahedron* **1974**, *30* (18), 3299−3302.

(27) Bos, E. S.; van der Doelen, A. A.; Rooy, N. v.; Schuurs, A. H. W. M. 3,3′,5,5′-Tetramethylbenzidine as an Ames Test Negative Chromogen for Horse-Radish Peroxidase in Enzyme-Immunoassay. *J. Immunoassay* **1981**, *2* (3−4), 187−204.

(28) Josephy, P. D.; Eling, T.; Mason, R. P. The horseradish peroxidase-catalyzed oxidation of 3,5,3′,5′-tetramethylbenzidine. Free radical and charge-transfer complex intermediates. *J. Biol. Chem.* **1982**, *257* (7), 3669−3675.

(29) Bally, R. W.; Gribnau, T. C. J. Some Aspects of the Chromogen 3,3,5,5-Tetramethylbenzidine as Hydrogen Donor in a Horseradish Peroxidase Assay. *Clin. Chem. Lab. Med.* **1989**, *27* (10), 791−795.

(30) Awano, H.; Ogata, T.; Murakami, H.; Yamashita, T.; Ohigashi, H. Radical salts as charge-transfer complexes between aromatic diamines and their diiminium cations. *Synth. Met.* **1990**, *36* (2), 263−266.

(31) Zhu, C.; Yang, H.; Cao, X.; Hong, Q.; Xu, Y.; Wang, K.; Shen, Y.; Liu, S.; Zhang, Y. Decoupling of the Confused Complex in Oxidation of 3,3′,5,5′-Tetramethylbenzidine for the Reliable Chromogenic Bioassay. *Anal. Chem.* **2023**, *95* (44), 16407−16417.

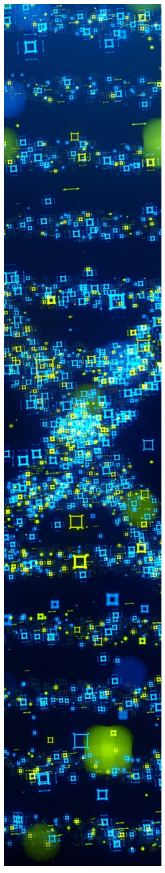

CAS BIOFINDER DISCOVERY PLATFORM™

STOP DIGGING THROUGH DATA —START MAKING DISCOVERIES

CAS BioFinder helps you find the right biological insights in seconds

Start your search

CAS
A division of the American Chemical Society

https://doi.org/10.1021/cbmi.5c00200
Chem. Biomed. Imaging XXXX, XXX, XXX−XXX